Article

Not peer-reviewed version

Photocatalytic Degradation of Azo Dyes over Magnetite-Based Catalyst: Kinetic, Thermodynamic and Structure-Activity Studies

Jackson Anderson S. Ribeiro , Júlia F. Alves , Bruno César Barroso Salgado , Alcineia C. Oliveira , Rinaldo S. Araújo , Enrique Rodríguez-Castellón *

Posted Date: 8 August 2024

doi: 10.20944/preprints202408.0535.v1

Keywords: heterogeneous photo-Fenton-like; magnetite; degradation; azo dyes; molecular effects

Article

Photocatalytic Degradation of Azo Dyes over Magnetite-Based Catalyst: Kinetic, Thermodynamic and Structure-Activity Studies

Jackson Anderson S. Ribeiro [1], Júlia F. Alves [1], Bruno César B. Salgado [2], Alcineia C. Oliveira [3], Rinaldo S. Araújo [1,*] and Enrique Rodríguez-Castellón [4,*]

[1] Departamento de Química e Meio Ambiente. Instituto Federal de Educação-IFCE, Campus de Fortaleza, Av. 13 de Maio, Fortaleza 60040-531, Ceará, Brazil; jacksons.anderson.sena07@aluno.ifce.edu.br (J.A.S.R.), julia.ferreira.alves08@aluno.ifce.edu.br (J.F.A.)

[2] Departamento de Química e Meio Ambiente. Instituto Federal de Educação-IFCE, Campus de Maracanaú, Av. Parque Central, Maracanaú, 61939-140, Ceará, Brazil; brunocesar@ifce.edu.br (B.C.B.S.)

[3] Departamento de Química Analítica e Físico-Química, Universidade Federal do Ceará, Campus do Pici, Bloco 940, Fortaleza 60455-760, Ceará, Brazil; alcineia@ufc.br (A.C.O.)

[4] Departamento de Química Inorgánica, Instituto Interuniversitario de Investigación en Biorrefinerías I3B, Facultad de Ciencias, Universidad de Málaga, 29071 Málaga, Spain

* Correspondence: castellon@uma.es (E.R.-C.); rinaldo@ifce.edu.br (R.S.A.)

Abstract: Textile wastewater containing dyes pose significant environmental hazards. Advanced oxidative processes, especially the heterogeneous photo-Fenton process, are effective in degrading a wide range of contaminants due to high conversion rates and ease of catalyst recovery. This study evaluates the photocatalytic degradation of azo dyes Acid Red 18 (AR18), Acid Red 66 (AR66) and Orange 2 (OR2) using magnetite as a catalyst. The magnetic catalyst was synthesized via a hydrothermal process at 150°C. Experiments were conducted at room temperature, investigating the effect of catalyst dosage, pH, and initial concentrations of H_2O_2 and AR18 dye. Kinetic and thermodynamic studies were performed at 25, 40 and 60°C for the three azo dyes (AR18, AR66 and OR2) and the effect of the dye structures on the photocatalytic efficiency was investigated. At 25 °C for 0.33 mmol.L^{-1} of dyes at pH 3.0, using 1.4 g.L^{-1} of catalyst and 60 mg.L^{-1} of H_2O_2 under a UV radiation of 16.7 mW.cm^{-2} the catalyst showed a 62,3% degradation for AR18, 79.6% for AR66, and 83.8% for OR2 in 180 minutes of reaction. The oxidation of azo dyes under these conditions is spontaneous and endothermic. The pseudo-first order kinetic constants indicated a strong temperature dependence with an order of reactivity of the type: OR2 > AR66 > AR18, which is associated to the characteristics of molecular complexity (size, steric hindrance, aromatic conjugation), electrostatic repulsion and the nature of the acid-base interactions on the catalytic surface.

Keywords: heterogeneous photo-Fenton-like; magnetite; degradation; azo dyes; molecular effects

1. Introduction

Due to environmental concerns, the global demand for lesser consumption of water and lowers discharge of industrial and domestic wastewater is a major challenge to environmental sustainability [1,2]. An important example is the consumption of excessive amounts of water and synthetic dyes by textile industrial processes, which constitutes harmful effects on human health and ecosystems, resulting in a huge amount of non-biodegradable organic compounds in the environment [2–4]. In this respect, hazardous wastewater treatment processes for removing organic pollutants are required to overcome their excess and improve the discharged water quality.

Efficient processes for rapid removal of organic contaminants, such the use of advanced oxidation processes (AOPs), have become ubiquitous in remediation methods for clean-up of wastewater by organic contaminants degradation to mitigate their adverse consequences on the

 doi:10.20944/preprints202408.0535.v1

environment [5,6]. Moreover, the state-of-the-art in AOPs process shows the chemical oxidation of dyes through *in situ* generation of highly reactive oxygen species e.g., hydroxyl radicals (•OH), superoxide radicals ($O_2^{\bullet-}$) and singlet oxygen ($^1O_2$) by mechanistic routes of photocatalysis, ozonation, electrocatalysis, oxidation by Fenton reaction, and Fenton-like processes [7–11]. One of the promising route for dyes degradation is the Fenton photocatalytic process, which has outstanding advantages for textile wastewater removal with rapid reaction rate and time [7,12,13]. Especially, the use of iron based catalysts in Fenton-like processes gives photogenerated electrons to rise the Fe^{3+}/Fe^{2+} conversion rate, while light is used for decolorization of dyes contaminants [13,14].

One of the difficulties associated with the utilization of the benchmark photo-Fenton catalysts such as α-Fe_2O_3, Fe_3O_4 and FeOOH among other iron-based oxides, is a high photogenerated electron-hole pair complexation rate, being considered to be a crucial factor that influences the low accessibility of the active sites and the light absorption efficiency of the catalytic performance in these processes [15–18]. It is acknowledged that the current state of Fe^{2+} ions present in magnetite is not yet sufficient to reliably assign H_2O_2 gives the aforesaid hydroxyl and hydroperoxyl radical ($HO_2^{\bullet}$) and/or superoxide radical anions to allow the oxidation of Fe^{2+} to Fe^{3+} along with the consumption of •OH radicals by the proper Fe^{2+} ion addressing high efficiencies to oxidize the organic pollutants [19].

On the other hand, it should be noted than use of magnetite as catalysts allow to reduce the unit operation and accelerate the recovery of the magnetic catalyst which makes wastewater treatment more inexpensive. The improvement of magnetite properties seems to be very promising for obtaining a highly stable catalyst during reactions for oxidative degradation of dyes at circumneutral pH [15–18].

Therefore, it is considered important to understand the magnetite properties to optimize the catalyst activity in heterogeneous photo-Fenton-like process for the oxidation of azo dyes, however, the effect of functional groups present in the dye molecule on the heterogeneous phase oxidation has been little explored in the literature. In the present study, the degradation kinetic and thermodynamic, the H_2O_2 and pollutant concentrations, pH, the catalyst amount and the relationship between the structures of the dyes and their photocatalytic characteristics were examined for the degradation de azo compounds e.g., Acid Red 18 (AR18), Acid Red 66 (AR66), and Orange 2 (OR2) on magnetite.

2. Results and Discussion

2.1. Heterogeneous Photo-Fenton-Like Reaction

Figure 1 shows the AR 18 azo dye photodegradation performances over the Fe_3O_4 catalyst. The effects of catalyst dosage in Fenton-like reaction on the degradation efficiency of AR 18 azo dye compared with other reaction systems are investigated.

Preliminary catalytic runs to analyze the catalyst dosage variations on the efficient degradation of AR 18 over magnetite catalyst are shown in Figure 1a. It may be noted that the AR18 degradation slight increase from 58 to 88% from catalyst dosage of 0.5 to 1.4 $g.L^{-1}$, when using an initial AR 18 of ca. 60 $mg.L^{-1}$ within 120 min, but that of 2.0 $g.L^{-1}$ is slightly decreases achieving 83%. The enhancement in degradation efficiency may be attributed to the combined effects of direct oxidation by UV light (photolytic mechanism) and the contribution of this radiation to the formation of •OH radicals via decomposition of H_2O_2 in an aqueous medium (photochemical mechanism) and/or on the surface of the catalyst (photocatalytic mechanism), according to equations 1 to 3. On the other hand, the slight reduction in catalytic activity for a dosage of 2.0 $g.L^{-1}$ may be associated with difficulty in penetrating light into the reaction medium due to the amount of catalyst in suspension. Nevertheless, such a rapid drop in the percentage degradation is not reflected in any alteration of the magnetite structure.

Blank runs conducted with 60 $mg.L^{-1}$ of AR 18 at pH 3.0 in 120 min using magnetite as catalyst reveal that the use of H_2O_2 and UV radiation alone results a degradation of the azo dye of less than 10%. Due to the absence of the catalyst, H_2O_2 and UV irradiation offer limitations to the reaction occurrence, where the AR18degradation is meaningless. Even though the photochemical process using UV/H_2O_2 without a catalyst may affect AR18 degradation with ~ 80% for 60 $mg.L^{-1}$ and ~ 45%

 doi:10.20944/preprints202408.0535.v1

for 200 mg.L^{-1} (Figure 1b), the activity is comparatively modest for a Fenton-like process in the presence of magnetite with maximum degradation of 95%, under the conditions used here.

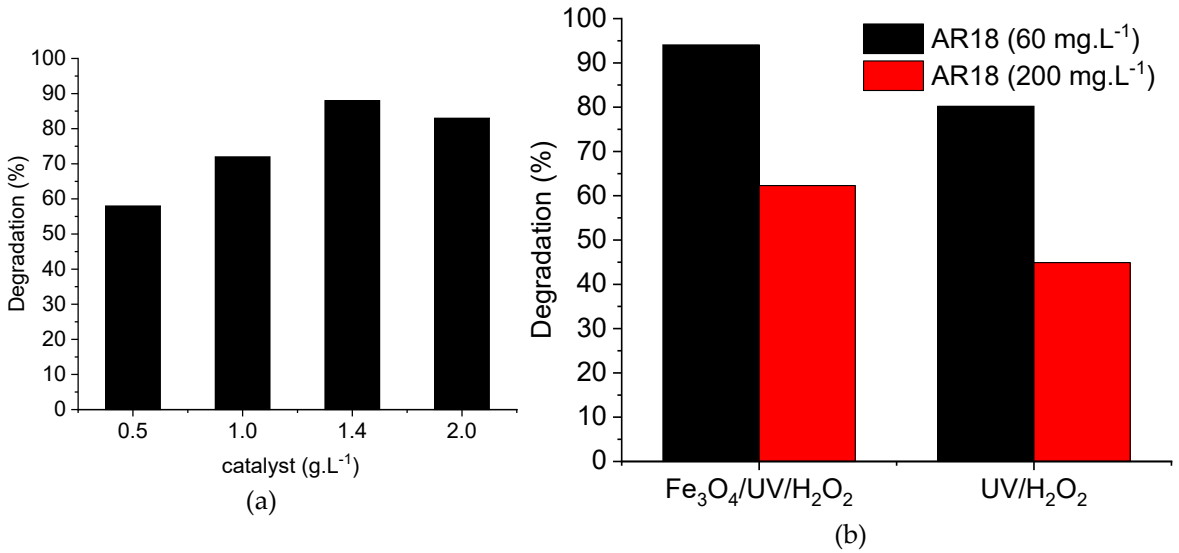

Figure 1. Effects of the AR18 degradation at 25 °C with I_L = 16.7 mW.cm^{-2}. (a) initial catalyst dosage using a C_0(AR18) of ca. 60 mg.L^{-1}, C_0(H_2O_2) of ca. 30 mg.L^{-1} at a pH of 3.0 during 120 min of reaction time. (b) Blank runs of the degradation of the AR18 over magnetite in distinct reaction conditions. C_0(Fe_3O_4) = 1.4 g.L^{-1}, C_0(AR18) = 60 mg.L^{-1}, C_0(H_2O_2) = 60 mg.L^{-1}, I_L = 16.7 mW.cm^{-2}, and a pH of 3.0 at 120 min.

Based on the abovementioned results, the catalyst dosage is set at 1.4 g.L^{-1} in the presence of H_2O_2/UV, which is suitable to undertake a systematic study of the AR18 azo dye photodegradation over the Fe_3O_4 as a catalyst. The effects of various Fenton-like reaction parameters on the AR 18 azo dye degradation efficiency are evaluated (Figure 2).

The influence of pH for Fenton and Fenton-like reaction as a parameter to elucidate the availability of Fe^{2+} to decompose H_2O_2 and generate the hydroxyl radicals in Fenton and Fenton-like reaction over iron-based catalysts with optimum pH in the range of 2.5-4.0 is evaluated [20–22].

The degradation efficiencies at the different pH tested are related to the zeta potential on the magnetite surface, which were + 8.4 mV at pH = 3.0, -6.26 mV at pH = 6.0 and -21.7 mV at pH = 8.0. The AR18 solution has an initial pH of 6 and under this condition the degradation efficiency is only 7.5% in 30 min of reaction, while a conversion of 32% can be achieved at pH = 3.0 for the same reaction time. After 60 min, the degradation efficiency improves and activities around 20% are only observed at natural pH (6.0) and slightly alkaline pH (8.0). On the contrary, at pH = 3.0 the degradation efficiency increases up to 60.3%. In 120 min, degradation efficiencies were 88% in acidic medium and approximately 39% and 38% at pHs = 6.0 and 8.0, respectively (Figure 2a). At pH 8.0 the magnetite catalyst is observed to be stable and there is no significant change in the degradation efficiency compared to that observed at almost neutral pH (pH = 6.0). In general, at pH values close to 3.5, azo dye molecules are effectively degraded by •OH radicals through the decomposition of H_2O_2 on the catalytic surface of magnetite [11]. Furthermore, the oxidation potential of the •OH /H_2O redox couple is greater at acidic pH values, which favors the degradation efficiency. At higher pH values (alkaline medium), the oxidizing effect decreases due to the reactions between •OH radicals and H_2O_2) [11,23]. Additionally, in an alkaline medium, the photocatalytic treatment of Acid Red 18 on WO_3 microspheres decorated with goethite showed a 16% reduction in degradation when the pH was increased from 1.89 to 9.64. This behavior was attributed to electronic repulsion between the anionic dye molecule and the $^-$OH groups attached to the catalyst surface, as can also be related in this study [24].

 doi:10.20944/preprints202408.0535.v1

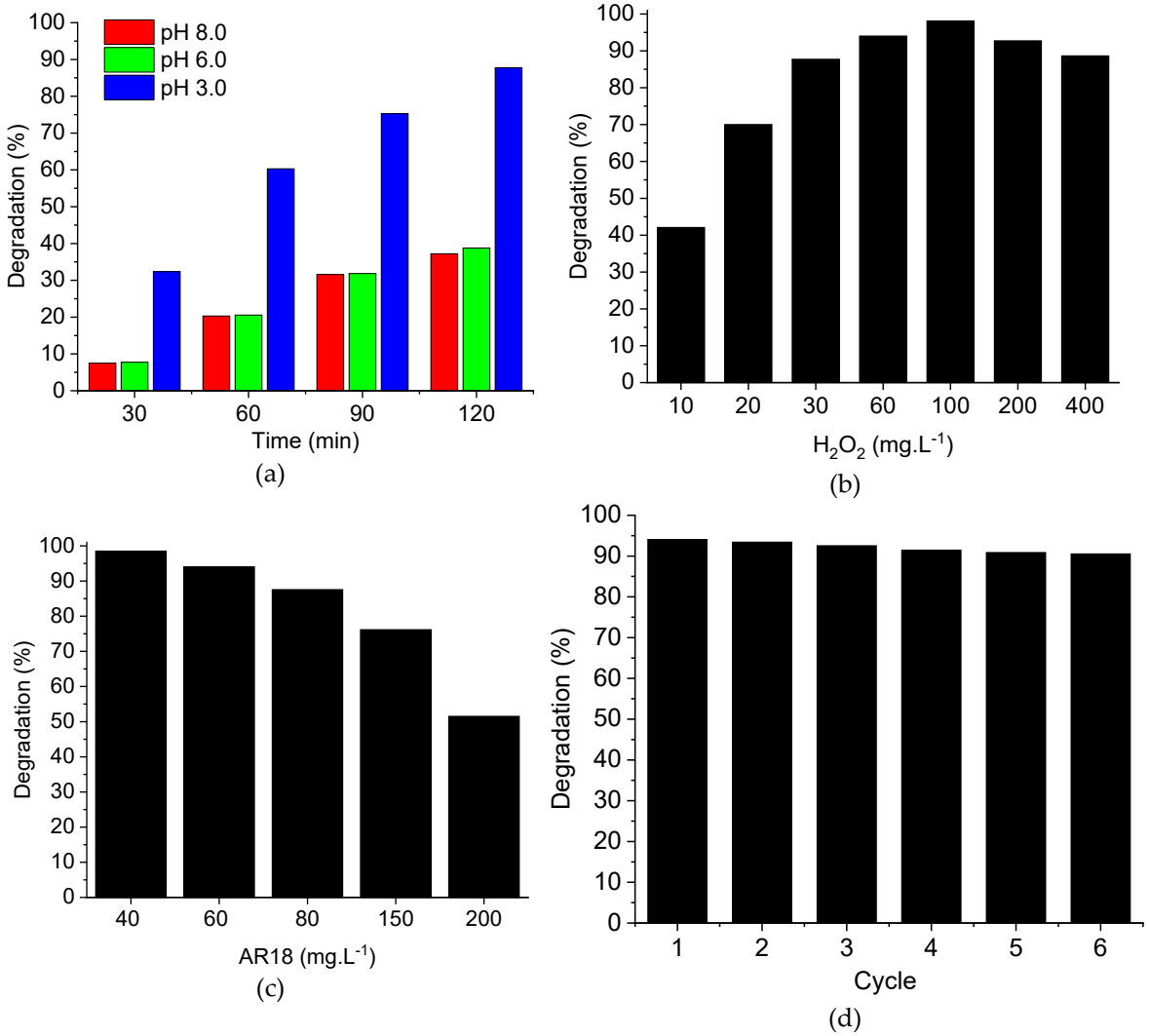

Figure 2. (a) Influence of the pH with an initial catalyst dosage $C_0(Fe_3O_4)$ of 1.4 g.L^{-1} at a fixed condition of C_0(AR18) = 60 mg.L^{-1}, $C_0(H_2O_2)$ equal to 30 mg.L^{-1} within 120 min. (b) Influence of the initial H_2O_2 concentration using $C_0(Fe_3O_4)$ of 1.4 g.L^{-1}, C_0(AR18) of about 60 mg.L^{-1} at a pH of 3.0 in 120 min. (c) C_0(AR18) effects with a $C_0(Fe_3O_4)$ of 1.4 g.L^{-1}, $C_0(H_2O_2)$ of 60 mg.L^{-1}, a pH of 3.0 and 120 min.(d) Reuse of the Fe_3O_4 at 25 °C after photo-Fenton reaction using a 1.4 g.L^{-1}, C_0(AR18) of 60 mg.L^{-1}, $C_0(H_2O_2)$ = 60 mg.L^{-1}, I_L = 16.7 mW.cm^{-2}, at a pH of 3.0 and t = 120 min.

Because of the initial H_2O_2 concertation greatly affects the AR18 degradation under acidic conditions [22], to understand the photocatalytic trend, a wide range of H_2O_2 concentrations should be considered. Figure 2b illustrates that the degradation of the azo dye increased linearly from 42.1 to 94.1% with H_2O_2 concentration increment in the range of 10-60 mg.L^{-1} within 120 min. With further initial H_2O_2 up to 100 mg.L^{-1}, the degradation efficiency diminished between 2.2% e 9.4%. This might seem counterintuitive, because larger amounts of H_2O_2 would likely generate more •OH radicals to degrade the azo dye, However, with an excess of H_2O_2, the rate of •OH recombination increases (•OH + •OH → H_2O_2) and the parallel reaction of •OH consumption by H_2O_2 is favored to form HO_2• or O_2^- (H_2O_2 + •OH → H_2O + HO_2•), which are less reactive species than •OH [25,26].

In addition, it is commonly accepted that the effect of azo dye concentration on Fenton and Fenton-like oxidations is limited at higher concentrations of AR18 due to the effective hydroxyl radicals formation on the magnetite catalyst [11,22,27]. Accordingly, Figure 2c shows a quite impressive almost complete AR18 degradation efficiency for a concentration below 80 mg.L^{-1}. As expected, the azo dye concentration between 150 and 200 mg.L^{-1} gives only 76.1% and 51.5% suggesting that Fe^{2+} species of magnetite can still be present, but its availability might be low, which may be related to the adsorption on the catalyst surface of several intermediate products formed

 doi:10.20944/preprints202408.0535.v1

during the oxidative process, including aromatic compounds, naphthalenes and their hydroxylated and nitrified derivatives, naphtodiols and phthalic acid derivatives [28]. Hence, with the chosen magnetite catalyst loading, 200 mg.L^{-1} was used for further kinetic and thermodynamics studies of AR18, AR16 and OR2.

The requirement for a stable catalyst in the Fenton-like reaction can be understood based on the recycling experiments. Figure 2d indicates that there are six cycles of consecutive uses of magnetite without any loss of degradation efficiency. At the end of the reaction, a steady state plateau about 90-94% is reached for the initial AR18 concentration of 60 mg.L^{-1}, at pH of 3.0 in 120 min, with no Fe species leaching as determined by AAS chemical analyses. These results are comparable to those in literature reports on spinel isostructural ferrite-based catalysts [11,29,30].

2.2. Kinetic and Thermodynamic of Degradation

According to the findings, reaction kinetics plays an important role in determining the rate of Fenton photocatalytic degradation processes [11,29].

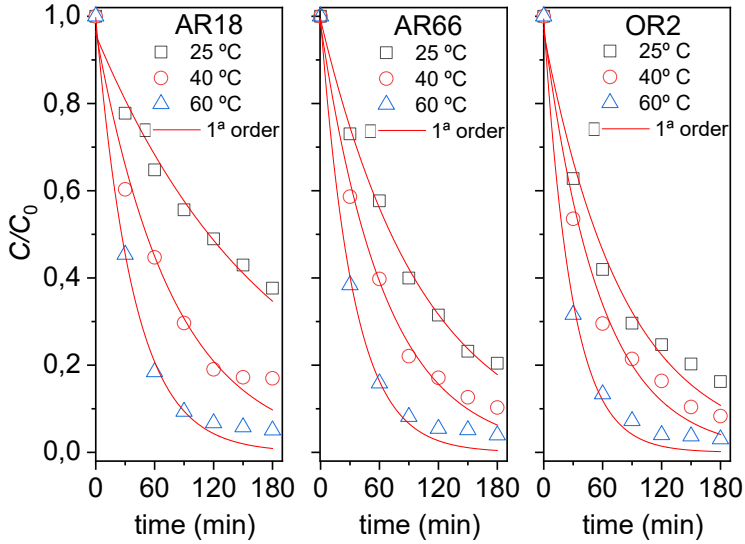

Figure 3. Degradation of AR18, AR66 and OR2 in a photo-Fenton-like process in function of time. Reaction conditions: $C_0(Fe_3O_4)$ = 1.4 g.L^{-1}, C_0(dye) = 0.33 mmol.L^{-1}, $C_0(H_2O_2)$ = 60 mg.L^{-1}, I_L = 16.7 mW.cm^{-2} and a pH of ca. 3.0.

The pseudo-first-order model was applied for the AR18, AR66 and OR2 azo des with similar structures. Figure 3 depicts the effect of reaction temperature in the range of 25–60 ◦C. At 25◦C,all azo dyes undergo higher degradation efficiency in shorter reaction time owing to elevated dye concentrations, evidencing a major collision rate between azo dyes and •OH radicals. With increasing of reaction temperature from 40 to 60 ◦C, an increment in reaction rate is observable for all azo dyes, at short reaction times. As the reaction proceeds, the degradation efficiency caused by the decreased collision rate between azo dyes intermediate compounds and hydroxyl radicals. In agreement, increased temperatures favor major collisions between the dye and OH radicals. In agreement, increased temperatures favor higher collisions between dye and OH radicals, although the rate is not affected with respect to the change in temperature within the range of longer reaction times [13,31,32]. The degradation of azo dyes follows the order: OR2 > AR66 > AR18, with the azo dye OR2 reacting with better efficiency at the three temperatures investigated.

The Arrhenius plots for the photo-Fenton degradation of azo dyes are depicted in Figure 4. The k_1 (min^{-1}) and E_a (kJ.mol^{-1}) parameters are given in Table 1. The Arrhenius plots of the natural logarithm *of* k_1 is linearly correlated with the reaction temperature, as shown in Figure 4.

Preprints.org (www.preprints.org) | NOT PEER-REVIEWED | Posted: 8 August 2024 doi:10.20944/preprints202408.0535.v1

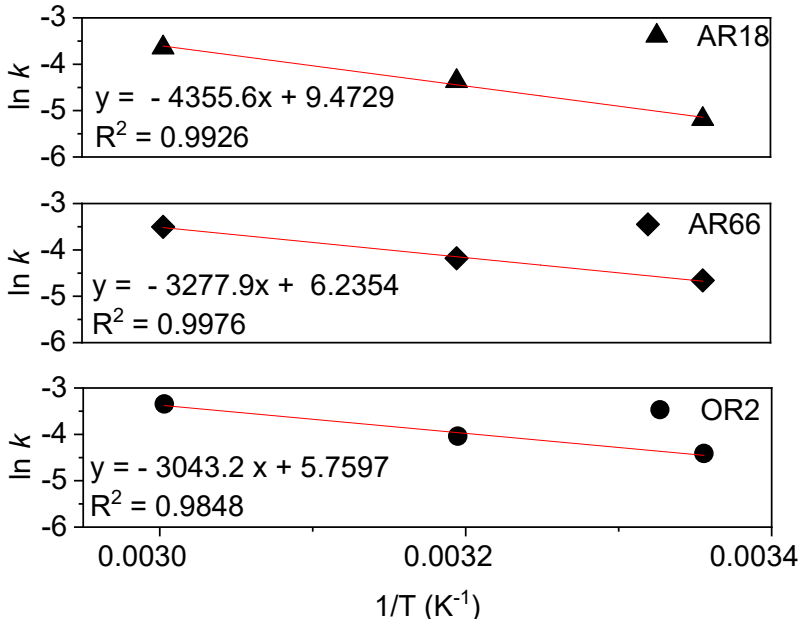

Figure 4. Arrhenius plots for photo-Fenton degradation of the AR18, AR66 and OR2. $C_0(Fe_3O_4)$ = 1.4 g.L^{-1}, C_0(dye) = 0.33 mmol.L^{-1}, $C_0(H_2O_2)$ = 60 mg.L^{-1}, I_L = 16.7 mW.cm^{-2} and a pH of ca. 3.0.

Photodegradation of the azo dyes on the magnetite surface is relied upon to improve the degradation efficiency. The examined kinetic data show a high correlation coefficient of 0.97 with a good fitting between calculated and experimental values suggesting that the Fenton-like process follows first order kinetics. In addition, the reaction rates of color removal and degradation efficiencies increase with increasing temperature, with the Fenton oxidation reaction being suitable. In fact, the activation energy of AR18 is 36.2 kJ.mol^{-1}, comparable with the degradation efficiency of Fe-based catalysts on Acid Red 18 azo dye in other studies [21,29,31–34]. For OR2, the calculated activation energy is 25.3 kJ.mol^{-1}, comparable with literature reports on magnetite-based catalysts [35–38]. These values indicate that the photocatalytic Fenton reaction rate can be controlled by the intrinsic kinetics at the surface of the magnetite catalyst.

Table 1. Pseudo first order rate constant and activation energy for AR18, AR66 and OR2 degradation via photo-Fenton process. $C_0(Fe_3O_4)$ = 1.4 g.L^{-1}, C_0(dye) = 0.33 mmol.L^{-1}, $C_0(H_2O_2)$ = 60 mg.L^{-1}, I_L = 16.7 mW.cm^{-2} and a pH of ca. 3.0.

T (°C)	AR18			AR66			OR2		
	k_1 (min^{-1})	R^2	E_a (kJ.mol^{-1})	k_1 (min^{-1})	R^2	E_a (kJ.mol^{-1})	k_1 (min^{-1})	R^2	E_a (kJ.mol^{-1})
25	0.0056	0.980		0.0095	0.997		0.0122	0.979	
40	0.0127	0.981	36.2	0.0153	0.992	27.2	0.0176	0.986	25.3
60	0.0262	0.994		0.0301	0.994		0.0353	0.994	

The parameter determination of Gibbs (ΔG), entropy (ΔS) and enthalpy (ΔH) for the AR18, AR66 and OR2 photodegradation, based on the van't Hoff equation in Figure 5. The obtained data are summarized in Table 2.

 doi:10.20944/preprints202408.0535.v1

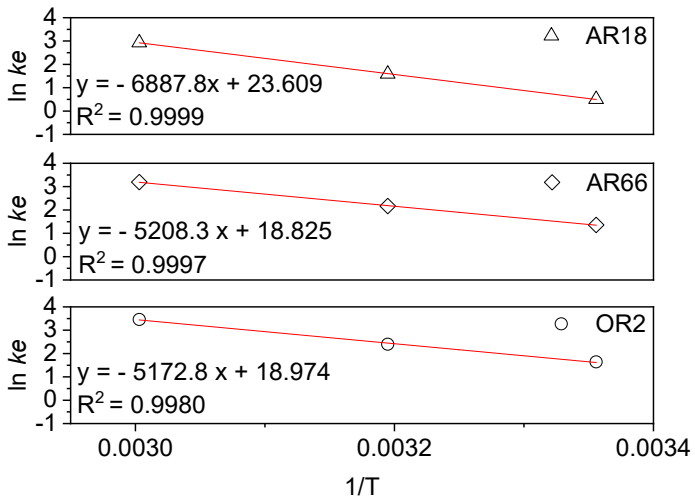

Figure 5. The van't Hoff plots for the photo-Fenton degradation of AR18, AR66 and OR2. $C_0(Fe_3O_4)$ = 1.4 g.L^{-1}, C_0(dye) = 0.33 mmol.L^{-1}, $C_0(H_2O_2)$ = 60 mg.L^{-1}, I_L = 16.7 mW.cm^{-2} and a pH of ca. 3.0.

The entalphy (ΔH) values obtained for the AR18, AR66 and OR2 azo dye are all similar to those of [39] , in the case of Acid Red 27. The ΔS values for AR18, AR66 and OR2 are 0.196, 0.157 and 0.158 kJ.mol^{-1}.K^{-1}, respectively, suggesting that the reaction is more spontaneous with increasing temperature [40]. The ΔG values for the OR2 degradation in the range of temperatures investigated are higher than those found for AR66 and AR18, which corroborates with the degradation order and the reaction kinetics (OR2 > AR66 > AR18).

Table 2. Thermodynamic parameters for AR18, AR66 and OR2 azo dye photo-Fenton degradation. $C_0(Fe_3O_4)$ = 1.4 g.L^{-1}, C_0(dye) = 0.33 mmol.L^{-1}, $C_0(H_2O_2)$ = 60 mg.L^{-1}, I_L = 16.7 mW.cm^{-2} at a pH of 3.0.

T (°C)	ΔH (kJ.mol^{-1})	ΔS (kJ.mol^{-1}K^{-1})	ΔG (kJ.mol^{-1})
		AR18	
25			-1.25
40	57.3	0.196	-4.13
60			-8.12
		AR66	
25			-3.37
40	43.3	0.157	-5.64
60			-8.84
		OR2	
25			-4.07
40	43.1	0.158	-6.25
60			-9.58

This behavior can be explained in terms of molecular effects related to the polar group natures, possible steric hindrance and, to some extent, to the type of the aromatic ring conjugation in the azo dye structure. OR2 and AR18 are hydroxyl azo aqueous species forming hydrazones (*o*-ortho and/or *p*-para), while AR 66 is typically an aminoazo dye where azo tautomeric arrangements predominate [41], despite the formation of the *o*-hydrazone in another molecular region.

Particularly, the OR2 azo dye occurs as an *o*-hydrazone (Figure 6a) without perturbation of the sulphonate group (-SO_3^-), which is *p*-substituted in the phenyl (ph), while in AR18 (Figure 6b), the *o*-hydrazone is protected or hindered by -SO_3^- at positions 2 and 4 of the naphtyl (naph) group adjacent to the azo bond, and there is a third -SO_3^- *p*-substituted group in the second naphtyl group of the molecule. Thus, the high number of sulphonyl groups in AR18 inhibits by electrostatic repulsion the •OH attack and the other reactive oxygen species (ROS) and reduce the steric hindrance and the accessibility the oxidizing radicals (•OH, $^1O_2$, $O_2^{\bullet-}$, $HO_2^{\bullet}$) to the azo groups and aromatic azo rings

 doi:10.20944/preprints202408.0535.v1

[42]. Under these conditions, OR2 is easily degraded by ROS generated on the Fe_3O_4 (≡Fe^{3+}) surface catalyst of AR18, as observed in the direct photodegradation of these dyes by UV irradiation in a rotating disk photoreactor [43]. In this direct photolysis, a pseudo-first order constant ratio for Orange 2 and Acid Red 18 (k_1 OR2/k_1 AR18) was 1.97, which is similar (~ 2.17) to that found in this work for photocatalytic degradation on synthesized magnetite. For AR66, the k_1 (min^{-1}) is between the k_1 for OR2 and AR18, which can be explained in function of the minor steric hindrance and electrostatic repulsion generated from two structural sulphonate situated in position 2 of the *o*-hydrazone and another *p*-substituted in the phenyl group associated with the second azo group of the molecule (Figure 6c). Besides, the conjugation of the rings increment in the disulphonate (AR66) type: naph-azo-ph-azo-ph is more favorable to photoconversions than the naph-azo-naph conjugation present in AR18 (trisulphonate).

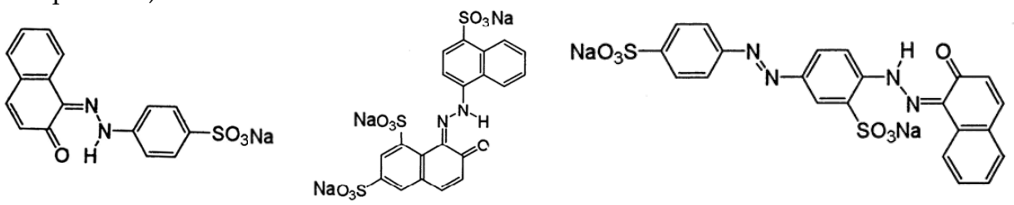

(**a**) OR2 (**b**) AR18 (**c**) AR66

Figure 6. Azo dye structures in a study adapted from worlddyevariety.com.

Based on the hard/soft acid/base (HSAB) of Pearson theory [44]; Fe^{3+} is typically a strong strength Lewis acid (HA) with high affinity for strong strength Lewis (HB), giving ionic interactions for base HA/HB complex interactions. On the other hand, azo dyes can be characterized as soft bases (SB) with a basic character decreasing with increasing carbonic chain length, which generates a diffuse electron distribution. Thereby, the minor molecular complexities (MC) and topological polar surface area (PSA) in the OR2 (MC = 529, PSA = 111 Å) and AR18 (MC = 958, PSA = 201 Å) in comparison with that of AR18 (MC = 1080, PSA = 242 Å) (data obtained from Pubchem databases) can favor the catalytic surface interactions, promoting the heterogeneous mechanistic oxidation. In this order, the polar covalent interaction features in the conjugated Fe^{3+}//OR2 complex are stronger than in than the Fe^{3+}//AR18 base system, whereas the Fe^{3+}//AR66 conjugated par appears as an intermediate character.

When considering the catalyst participation in the processes, it is important to figure out the position and nature of the two active iron species on the surface (≡Fe^{3+} and/or ≡Fe^{2+}) in contact with the reactive functional groups (-N=N-, -SO_3^-, -C=C-) of the excited dye molecule (dye*). The heterogeneous photo-Fenton process is described by the following equations (Eq.1 to 6), being the •OH generation due to the H_2O_2 direct photolysis at 180-340 nm (photochemistry reaction, Eq. 2) and iron cations (photocatalytic reactions, Eq. 3 and 4) [3,15,45].

$$dye + h\lambda \rightarrow dye^* \quad (1)$$

$$H_2O_2 + h\lambda \rightarrow 2\ {}^{\bullet}OH \quad (2)$$

$$\equiv Fe^{3+} + H_2O_2 + h\lambda \rightarrow \equiv Fe^{2+} + {}^{\bullet}OH + H^+ \quad (3)$$

$$\equiv Fe^{2+} + H_2O_2 \rightarrow \equiv Fe^{3+} + {}^{\bullet}OH + {}^{-}OH \quad (4)$$

$$\equiv Fe^{2+} + H_2O_2 \rightarrow \equiv Fe^{3+}\text{-}OH + {}^{-}OH \quad (5)$$

$$dye^*\ (organic) + {}^{\bullet}OH \rightarrow products \quad (6)$$

Magnetite synthesized is a magnetic mixture of hematite (α-Fe_2O_3), maghemite (γ-Fe_2O_3) and goethite (α-FeOOH) having about 70% of Fe_3O_4 and 30% of the aforesaid phases [46]. Such composition is non-stoichiometric and is abundant in iron species that act favorably in the •OH radical formation. Figure 7 show a comparison of the AR 18 degradation using various iron oxides

 doi:10.20944/preprints202408.0535.v1

with different Fe^{3+}/Fe^{2+} molar ratios, for instance, wüstite (FeO, Fe^{3+}/Fe^{2+}= 0), goethite (FeOOH, Fe^{3+}/Fe^{2+}= ∞), hematite (Fe_2O_3, Fe^{3+}/Fe^{2+}= ∞) and magnetite (Fe_3O_4, Fe^{3+}/Fe^{2+}= 4) prepared in this study.

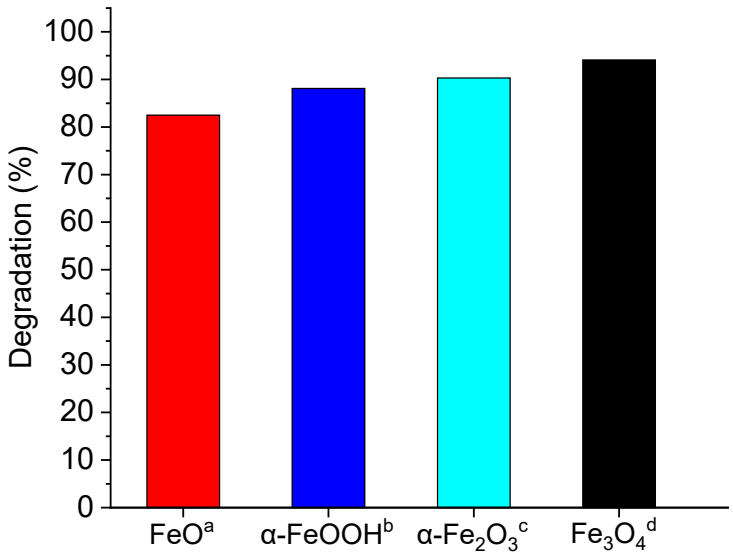

Figure 7. Comparison of the degradation efficiency of the AR18 azo dye at 25 °C over distinct iron catalysts via photo-Fenton process. Catalyst dosage of 1.4 $g.L^{-1}$, C_0(AR18) = 60 $mg.L^{-1}$, $C_0(H_2O_2)$ = 60 $mg.L^{-1}$, I_L = 16.7 $mW.cm^{-2}$, and a pH of 3.0 at t = 180 min. [a]Synthesized according to [47], [b]Synthesized according to [48], [c]Commercial (Sigma-Aldrich) and [d]synthesized in this work.

At 25 °C, the initial concentration of 60 $mg.L^{-1}$ of the dye is not a limiting factor for the catalytic activity of the various iron oxides (Figure 10), as observed for example at the concentration of 200 $mg.L^{-1}$ (0.33 $mmol.L^{-1}$) of Acid Red 18, where the maximum degradation was 62.3% (Figure 1b). The similar degradations indicate similar mechanistic considerations for catalytic surface, despite the oxy (hydroxide) nature of goethite, the major Fe^{3+} proportion seem to contribute to a slight higher oxidation to that of FeO, possessing only Fe^{2+} sites. In photo-Fenton systems with high Fe^{2+} concentrations under acidic conditions, Fe^{2+} exists in the $Fe(OH)^{2+}$ form, which determines a lower •OH radical generation and the decrease of the degradation rate [49].

2.3. Treated Solution Characterization

Figure 8 shows the UV-Vis spectra of the OR2 azo dye treatment, after the heterogeneous photo-Fenton reaction over the synthesized Fe_3O_4. The structural iron reacts with H_2O_2 giving rise to •OH radicals, which attacks the azo (-N=N-) groups producing an effective solution decolorization in 90 min of photocatalytic reaction. The UV decolorization at 230 nm and 310 nm is related to the benzene, naphthalene ring as shown in literature reports, although these bands have a much lower and slower intensity than the chromophore band positioned at 505 nm. These behaviors are similar to those observed in the degradation of the azo dyes Reactive Black 5 [50] and Orange 2 [51], indicating a high decolorization of the OR2 accompanied by a relative concentration of the residual compounds after the oxidative reactions. Regarding the chemical oxygen demand (COD) before and after the photo-Fenton reaction, only a reduction of 29.7% in chemical oxidation of organic matter, which is similar to the COD of 27% found in the degradation of the dye Acid Red 73 by heterogeneous photo-Fenton process [52]. These results reveal the need for long reaction times or harsh treatment conditions aiming the mineralization of the refractory compounds produced.

 doi:10.20944/preprints202408.0535.v1

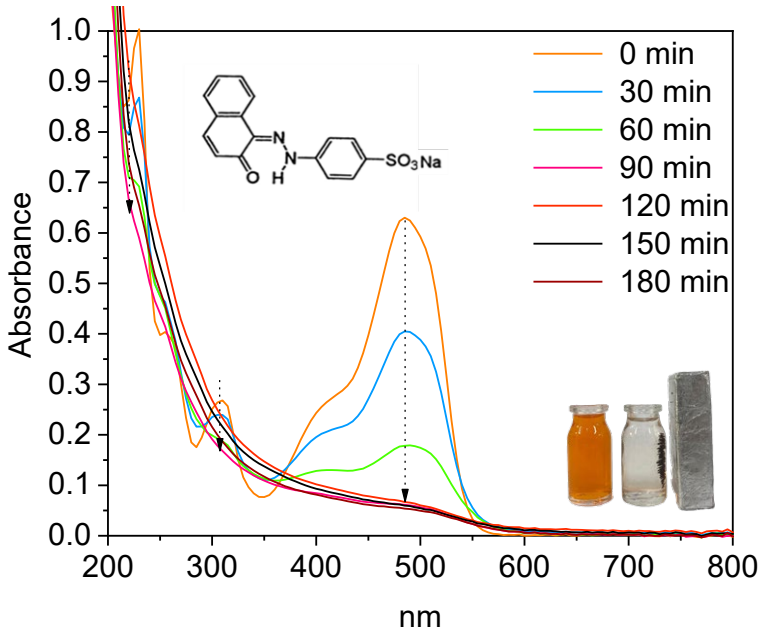

Figure 8. UV–Vis spectra of Orange 2 as a function of reaction time for OR2 at 60 °C in photo-Fenton-like processes. Catalyst dosage of 1.4 g.L^{-1}, C_0(dye) = 0.33 mmol.L^{-1}, C_0(H_2O_2) = 60 mg.L^{-1}, I_L = 16.7 mW.cm^{-2} at a pH of 3.0.

2.4. Spent Magnetite Characterization

The fresh magnetite characterizations are given in our previous reports [46]. XPS spectra of fresh and spent magnetite after the poto-Fenton-like reaction are shown in Figure.9. The XPS spectrum of fresh Fe_3O_4 (Figure 9a) is depicted with the main spin-orbit split peaks located at 710.2 and 724.9 eV (Table 3) for the doublet Fe $2p_{3/2}$ - $Fe_{5/2}$, respectively. These doublet peaks arise along with their shake-up satellites typically confirming that the magnetite has Fe species in both divalent Fe^{3+} and Fe^{2+} states [53]. Accordingly, the peak at about 710.8 eV is assigned to the Fe^{3+} ions in octahedral sites whereas that located at 723.9 eV indicates the presence of the Fe^{2+} species [54].

The recorded O 1s core level has three different oxygen species and a major contribution at 529.6 eV corresponds to 63%, due to the existence of lattice oxygens from the Fe-O bonds in Fe_3O_4,as previously detected in the literature [55]. This contribution is accompained by two other weak components near 531.0 eV (29%) from OH groups of physisorbed water molecules and 532.7 eV (8.0%) agreeing well with carbon bonded to oxygen species e.g., C–O and C=O [46,54].

Moreover, Fe^{3+}/Fe^{2+} atomic composition obtained from area ratio between the peak at 711.2 and 710 eV is 2.3 (Table 3) suggests the distribution of Fe^{3+} and Fe^{2+} ions between the different sites of magnetite, which has highly oxidized surface [46]. The C 1s core level appears with binding energies ascribed to –C=C– and adventitious carbon as the dominant peak at 284.7 eV (82%) along with peaks at C–OH at 286.0 eV (12%) and C–C=O– at 288.3 eV (6%), in agreement with the findings [53–56].

Preprints.org (www.preprints.org) | NOT PEER-REVIEWED | Posted: 8 August 2024 doi:10.20944/preprints202408.0535.v1

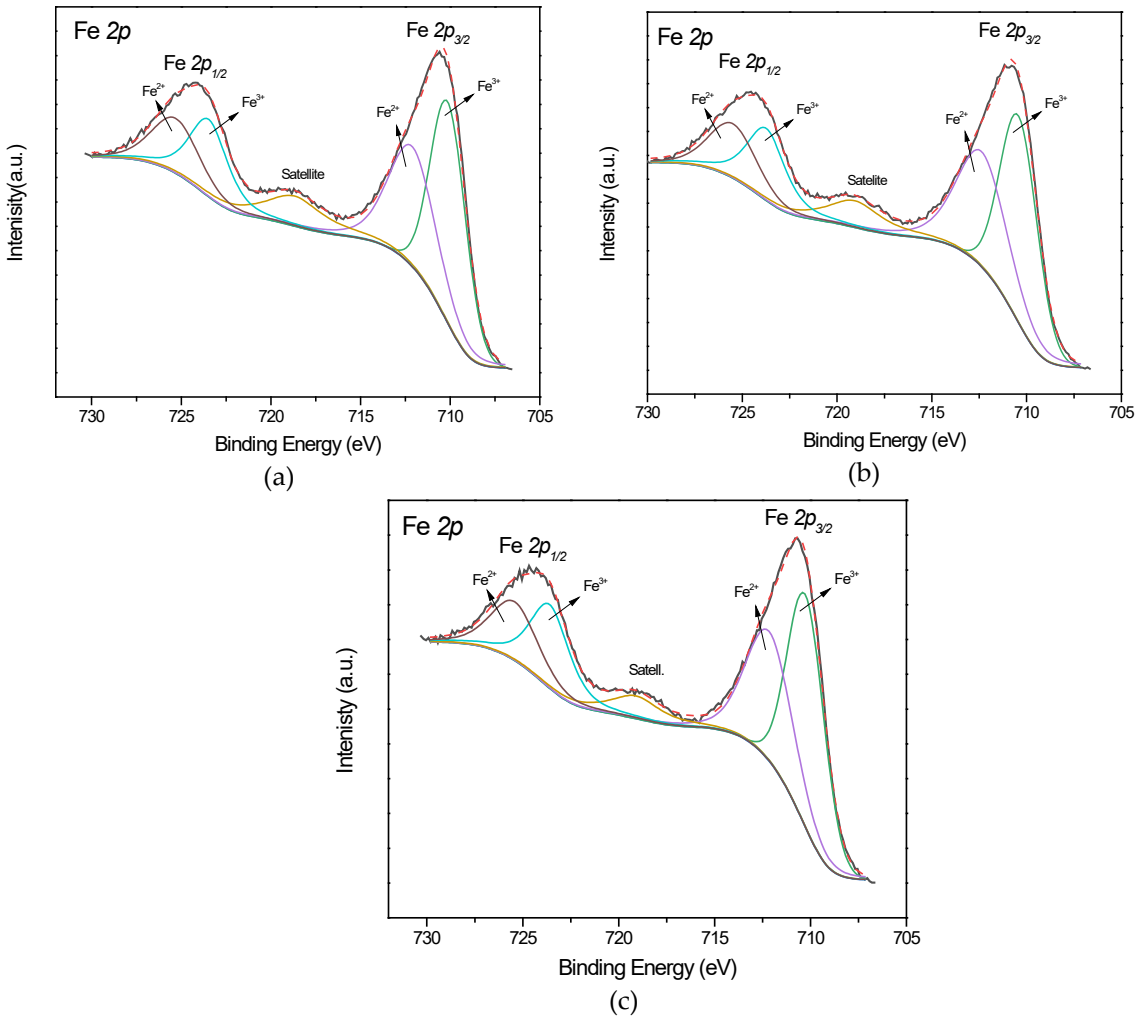

Figure 9. XPS spectra of Fe 2*p* core levels for magnetite. (a) fresh Fe_3O_4, and after photo-Fenton-like reaction with (b) AR18 and (c) AR 66. Reaction conditions: Catalyst dosage of 1.4 $g.L^{-1}$, C_0(dye) = 0.33 $mmol.L^{-1}$, $C_0(H_2O_2)$ = 60 $mg.L^{-1}$, I_L = 16.7 $mW.cm^{-2}$ at a pH of 3.0 at 60 °C.

These species arises from the incomplete organic precursors removal, even after the calcination of the solid.

To further verify the surface stability of the magnetite, the AR18 and AR66 azo dyes are degraded upon the photocatalytic Fenton-like reaction. Table 3 summarizes the binding energies of the magnetite after the catalytic reaction with the dyes. The XPS spectra of the magnetite after photo-Fenton-like reaction with AR18 and AR66 (Figures 9b and 9c) show similar results indicating that the valence states of iron is not changed after the title reaction. Similarly, C 1*s* and O 1*s* core levels have comparable values with those of the fresh magnetite, after dye degradation (Table 3). Moreover, the expected N 1*s* core level for Fe_3O_4/AR18 and Fe_3O_4/AR66 with binding energy close to 400 eV is not found after the reaction [46]. It could be associated with the weak chemisorption of the nitrogen groups of the dye on the sample.

In particular, the S 2*p* core level appears only for Fe_3O_4/R66, having binding energy at 168.1 eV due to S-O groups [46]. Additionally, the detected sulfates species on the surface of magnetite after AR66 Fenton-like reaction would contribute to the physisorption of the Fe active sites on magnetite providing a low performance of the solid with using the AR66 dye.

Table 3. XPS parameters of the fresh and spent magnetite after reaction with AR 18 and AR 66 dyes. Reaction conditions: Catalyst dosage of 1.4 $g.L^{-1}$, C_0(dye) = 0.33 $mmol.L^{-1}$, $C_0(H_2O_2)$ = 60 $mg.L^{-1}$, I_L = 16.7 $mW.cm^{-2}$ at a pH of 3.0 at 60 °C .

Sample	**Binding energy (eV)**

 doi:10.20944/preprints202408.0535.v1

	Fe 2$p_{3/2}$	Fe 2$p_{1/2}$	C 1s	O 1s	S 2p	Fe^{3+}/Fe^{2+} ratio
Fe_3O_4 [46]	710.0 (18)	724.9 (17)	284.7(82) 286.0(12) 288.3(6)	529.6(63) 531.0(29) 532.7(8)		2.3
Fe_3O_4/AR18	710.3 (17)	724.8 (23)	284.8(80) 285.3(12) 288.5(8)	529.9(63) 531.4(28) 532.7(9)		2.6
Fe_3O_4/AR66	710.2 (19)	724.7 (21)	284.8(81) 285.3(13) 288.6(6)	529.8(56) 531.4(28) 532.8(16)	168.1	2.4

The atomic concentration percentages of Fe, C and O in fresh Fe_3O_4 are 29.3, 56.5 and 14.4%. Comparison with the atomic concentrations of the components of the two dyes show values of C: 41.5%, O: 45.7%, Fe: 12.6% and C: 37.5%, O: 51.6%, Fe: 10.8%, S: 0.18% for Fe_3O_4/AR18 and Fe_3O_4/AR66 with deviations within the limits of precision and accuracy of the XPS technique.

Besides, Table 3 indicates that the Fe^{3+}/Fe^{2+} atomic ratio involves a 2.4-2.6 range for both dyes, which might be expected, according to the surface composition of magnetite [57]. It suggests the magnetite stability towards the reaction.

3. Materials and Methods

3.1. Materials

Pure Acid Red 18 ($C_{20}H_{11}N_2Na_3O_{10}S_3$, 604.48 $g.mol^{-1}$) azo dye was purchased from Acros Organics. Orange 2 ($C_{16}H_{11}N_2NaO_4S$, 85%, 350.32 $g.mol^{-1}$) and Acid Red 66 ($C_{22}H_{14}N_4Na_2O_7S_2$, 55%, 566.48 $g.mol^{-1}$) azo dyes were obtained from Sigma-Aldrich. All azo dyes reagents were used without further purification. The hydrogen peroxide solution (H_2O_2, 30 wt. %) was purchased from Êxodo Científica. Prior to the use, the content of H_2O_2 was evaluated by permanganate method [58]. The sulfuric acid (H_2SO_4, 98%) was obtained from Vetec. Deionized water was used in all experiments.

3.2. Catalyst Synhesis and Characterizations

Fe_3O_4 consisting primarily of a Fe^{3+}/Fe^{2+} molar ratio of 4 and was synthesized by a coprecipitation method, as found elsewhere [46,59]. The zeta potential and the particle size distributions at pH of 3.0, 6.0 and 8.0 were performed in a Zetasizer Nano S apparatus form Malvern.

The surface compositions and valence state of the elements present in the spent samples used at distinct reaction conditions were determined by X-ray photoelectron spectroscopy (XPS). XPS spectra were obtained on a PHI Versa-Probe II Scanning XPS Microprobe from Physical Electronics. The incident radiation was generated by the Al Kα X-ray source, operating at 1486.6 eV and 15 kV. The spectra were calibrated using the binding energy peak of C 1s at 284.8 eV from adventitious carbon.

3.3. Heterogeneous Photo-Fenton-Like Oxidation

The photocatalytic activity of the magnetite was conducted in a borosilicate reactor (height of ca. 13 cm; diameter of 6.5 cm) with a capacity of about 45 mL coupled to a circulating water jacket to maintain solution temperature. A UV-C Philips TUV PL-S 7W/2P model lamp of ca. 7.1 W was positioned to the reaction reactor. The aforesaid lamp generated UV irradiation at 254 nm with a radiation intensity (I_L) of ca. 16.7 $mW.cm^{-2}$.

Typically for photo-Fenton-like batch experiments, the reaction was initiated by introducing the H_2O_2 solution along of the azo dyes to the reaction system. Then, air flow at a 180 ± 20 $mL.min^{-1}$ rate was introduced in the system, which was used to have a homogeneous solution. The abovementioned suspension was exposed to UV-C lamp and aliquots were withdrawn to determine the concentration

 doi:10.20944/preprints202408.0535.v1

of the azo dyes solution by a UV-Vis spectrophotometer. When using Acid Red 18 (AR18) as reactant, the pH, initial concentration of H_2O_2 and an initial concentration of the AR18 azo dye were evaluated at 25 °C. Other azo dyes such as AR66 and OR2 having an initial concentration of ca. 0.33 mmol.L^{-1} were also examined. The calibration curve of each azo dye was set at 505, 510 and 485 nm for AR18, AR66 and OR2, respectively, using a Thermo Fisher UV-Vis Genesys 10 S spectrophotometer. Iron concentrations in solution were estimated by atomic absorption spectrophotometry using a Thermo Scientific AAS iCE 3000 equipment.

The effects of initial concentration azo dye, H_2O_2 initial concentration, catalyst dosage, pH besides kinetic and thermodynamic parameters were evaluated. Besides, initial dosage of catalyst was taken from literature reports [51,60].

The photo-Fenton catalytic degradation percentage was measured, as follows (Eq. 7):

$$\% \text{ Degradation } = \left(\frac{C_0 - C_t}{C_0}\right) * 100 \quad (7)$$

where: C_0 (mmol.L^{-1}) and C_t (mmol.L^{-1}) are the initial and final azo dyes concentrations at a given period, respectively.

To understand the Acid Red 18 azo dye at 25, 40 and 60 °C degradation kinetics, the pseudo-first-order kinetic model were used, according to the equation 8 [34]:

$$C = C_0 e^{-k_1 t} \quad (8)$$

where: C_0 is the initial concentration of AR18 (mmol.L^{-1}), C is the AR18 concentration (mmol.L^{-1}) at a certain reaction time t (min) and k_1 (min^{-1}) is the rate constant for pseudo-first-order reaction.

The activation energy (E_a, kJ.mol^{-1}) of the AR18, AR66 and OR2 l studied azo dyes was determined by the Arrhenius equation (Eq. 9), as reported in a previous [40]:

$$k_1 = \text{Ae}^{\frac{-Ea}{RT}} \quad (9)$$

where: A is the Arrhenius constant, k_1 is the rate constant for pseudo-first-order reaction, T is the absolute (K) and R is the universal constant of the gases (8.314 J.mol^{-1}.K^{-1}).

The variations of free Gibbs energy (ΔG), entropy (ΔS) and enthalphy (ΔH) themodynamics were determined according to the van't Hoff equations [61].

$$k_e = \frac{C_{\text{Ae}}}{C_{\text{Se}}} \quad (10)$$

$$\Delta G° = -RT \ln k_e \quad (11)$$

$$\ln k_e = \frac{\Delta S°}{R} - \frac{\Delta H°}{RT} \quad (12)$$

where: k_e is the equilibrium constant and C_{Ae} and C_{Se} are the degraded and remained azo dyes concentrations in the equilibrium, respectively.

4. Conclusions

The synthesized magnetite showed high photocatalytic efficiency for the degradation of dyes AR18, AR66 and OR2 under optimal conditions of 1.4 g.L^{-1} of catalyst, 60 mg.L^{-1} of H_2O_2, pH = 3.0 and radiation intensity of 16.7 mW.cm^{-2}. The material showed no decrease in catalytic activity after six consecutive reaction cycles, confirming its high stability, as observed by the XPS results. The kinetics were typically first order while the reactional thermodynamics confirmed spontaneous and endothermic degradation processes. Among the dyes, the OR2 molecule was the most easily degraded due to its lower structural complexity, lower steric hindrances and lower electrostatic repulsion with reactive oxygen species on the catalyst surface. This study showed the promising nature of photo-Fenton technology using magnetite as a catalyst in the treatment of aqueous solutions contaminated with azo dyes, also allowing to discuss and explain the effect of some chemical characteristics of the target molecule on the performance of oxidative degradation.

Author Contributions: Conceptualization, formal analysis, R.S.A.; methodology, J.A.S.R, J.F.A.; investigation, R.S.A; methodology, B.C.B.S.; writing—original draft preparation, writing—review and editing, funding acquisition, A. C. O., R.S.A. and E.R.-C.

Funding: The authors acknowledge the financial support from the Ministerio de Ciencia e Innovación, Spain (Grant TED2021-130756B-C31 MCIN/AEI/10.13039/501100011033) and "ERDF A way of making Europe" by the European Union NextGenerationEU/PRTR.

Data Availability Statement: The data presented in this study are available upon request from the corresponding authors.

Acknowledgments: J.A.S.R acknowledges the financial support for his master scholarship from the Conselho Nacional de Desenvolvimento Científico Tecnologico (CNPq), Brazil. Jose Vitor do carmo is grateful acknowledged by his contributions in this manuscript.

Conflicts of Interest: The authors declare no conflicts of interest.

References

1. Chen, Z., Yan, Y., Lu, C., Lin, X., Fu, Z., Shi, W., Guo, F. Photocatalytic self-Fenton system of g-C_3N_4-Based for degradation of emerging contaminants: a review of advances and prospects. *Molecules* **2023**, 28(15), 5916. https://doi.org/10.3390/molecules28155916
2. Zhang, Z., Bai, Z., Yu, S., Meng, X., Xiao, S. Photo-Fenton efficient degradation of organic pollutants over S-scheme ZnO@NH_2-MIL-88B heterojunction established for electron transfer channel. *Chem. Eng. Sci.* **2024**, 288, 119789.
3. Magomedova, A., Isaev, A., Orudzhev, F., Sobola, D., Murtazali, R., Rabadanova, A., Shabanov, N. S., Zhu, M., Emirov, R., Gadzhimagomedov, S., Alikhanov, N., Kasinathan, K. Magnetically separable mixed-phase α/γ-Fe_2O_3 catalyst for photo-Fenton-like oxidation of Rhodamine B. *Catalysts* **2023**, 13(5), 872. https://doi.org/10.3390/catal13050872
4. Nchimi Nono, K., Vahl, A., Terraschke, H. Towards high-performance photo-Fenton degradation of organic pollutants with magnetite-silver composites: synthesis, catalytic reactions and in situ insights. *Nanomaterials* **2024**, 14(10), 849. https://doi.org/10.3390/nano14100849
5. Feijoo, S., González-Rodríguez, J., Fernández, L., Vázquez-Vázquez, C., Feijoo, G., Moreira, M. T. Fenton and photo-Fenton nanocatalysts revisited from the perspective of life cycle assessment. *Catalysts* **2020**, 10(1), 23. https://doi.org/10.3390/catal10010023
6. Ismail, G. A., Sakai, H. Review on effect of different type of dyes on advanced oxidation processes (AOPs) for textile color removal. *Chemosphere* **2022**, 291, 132906. https://doi.org/10.1016/j.chemosphere.2021.132906
7. Dong, C., Fang, W., Yi, Q., Zhang, J. A comprehensive review on reactive oxygen species (ROS) in advanced oxidation processes (AOPs). *Chemosphere* **2022**, 308, 136205. https://doi.org/10.1016/j.chemosphere.2022.136205
8. Mahbub, P., Duke, M. Scalability of advanced oxidation processes (AOPs) in industrial applications: a review. *J. Environ. Manag.* **2023**, 345, 118861. https://doi.org/10.1016/j.chemosphere.2022.136205
9. Vorontsov, A. V. Advancing Fenton and photo-Fenton water treatment through the catalyst design. *J. Hazard. Mater.* **2019**, 372(1), 103-112. https://doi.org/10.1016/j.jhazmat.2018.04.033
10. Li, N., He, X., Ye, J., Dai, H., Peng, W., Cheng, Z., Yan, B., Chen, G., Wang, S. H_2O_2 activation and contaminants removal in heterogeneous Fenton-like systems. *J. Hazard. Mater.* **2023**, 458, 131926. https://doi.org/10.1016/j.jhazmat.2023.131926
11. Unal, B. O.; Bilici, Z.; Ugur, N.; Isik, Z.; Harputlu, E.; Dizge, N.; Ocakoglu, K. Adsorption and Fenton oxidation of azo dyes by magnetite nanoparticles deposited on a glass substrate. *J. Water Process Eng.* **2019**, 32, 100897. https://doi.org/10.1016/j.jwpe.2019.100897
12. Tunç, S., Gürkan, T., Duman, O. On-line spectrophotometric method for the determination of optimum operation parameters on the decolorization of Acid Red 66 and Direct Blue 71 from aqueous solution by Fenton process. *Chem. Eng. J.* **2012**, 181–182, 431-442. https://doi.org/10.1016/j.cej.2011.11.109
13. Rubeenaa, K. K., Reddy, P. H. P., Laiju, A. R., Nidheesh, P. V. Iron impregnated biochars as heterogeneous Fenton catalyst for the degradation of Acid Red 1 dye. *J. Environ. Manag.* **2018**, 226, 320-332. https://doi.org/10.1016/j.jenvman.2018.08.055
14. Sharma, M., Tyagi, V. V., Chopra, K., Kothari, R., Singh, H. M., Pandey, A. K. Advancement in solar energy-based technologies for sustainable treatment of textile wastewater: reuse, recovery and current perspectives. *J. Water Process Eng.* **2023**, 56, 104241. https://doi.org/10.1016/j.jwpe.2023.104241
15. Rusevova, K., Kopinke, F. D., Georgi, A. Nano-sized magnetic iron oxides as catalysts for heterogeneous Fenton-like reactions-influence of Fe(II)/Fe(III) ratio on catalytic performance. *J. Hazard. Mater.* **2012**, 241-242, 433-440. https://doi.org/10.1016/j.jhazmat.2012.09.068

16. Minella, M., Marchetti, G., De Laurentiis, E., Malandrino, M., Maurino, V., Minero, C., Vione, D., Hanna, K. Photo-Fenton oxidation of phenol with magnetite as iron source. *Appl. Catal. B Environ.* **2014**, 154–155, 102-109. https://doi.org/10.1016/j.apcatb.2014.02.006
17. Xia, P., Zhang, H., Ye, Z. Recent advances in the application of natural iron and clay minerals in heterogeneous electro-Fenton process. *Curr. Opin. Electrochem.* **2024**, 46, 101495. https://doi.org/10.1016/j.coelec.2024.101495
18. Muzenda, C., Arotiba, O. A. Improved magnetite nanoparticle immobilization on a carbon felt cathode in the heterogeneous electro-Fenton degradation of Aspirin in wastewater. *ACS Omega* **2022**, 7, 19261-19269. https://doi.org/10.1021/acsomega.2c00627
19. Yan, J., Yang, L., Qian, L., Han, L., Chen, M. Nano-magnetite supported by biochar pyrolyzed at different temperatures as hydrogen peroxide activator: synthesis mechanism and the effects on ethylbenzene removal. *Environ. Pollut.* **2020**, 261, 114020. https://doi.org/10.1016/j.envpol.2020.114020
20. Kang, Y. W., Hwang, K. Y. Effects of reaction conditions on the oxidation efficiency in the Fenton process. *Water Res.* **2000**, 34(10), 2786-2790. https://doi.org/10.1016/S0043-1354(99)00388-7
21. Barbusiński, K., Majewski, J. Discoloration of azo dye Acid Red 18 by Fenton reagent in the presence of iron powder. *Pol. J. Environ. Stud.* **2003**, 12(2), 151-155.
22. Malakootian, M., Moridi, A. Efficiency of electro-Fenton process in removing Acid Red 18 dye from aqueous solutions. *Process Saf. Environ. Prot.* **2017**, 111, 138-144. https://doi.org/10.1016/j.psep.2017.06.008
23. Hassani, A., Karaca, C., Karaca, S., Khataee, A., Açisli, Ö., Yilmaz, B. Enhanced removal of Basic Violet 10 by heterogeneous sono-Fenton process using magnetite nanoparticles. *Ultrason. Sonochem.* **2018**, 42, 390-402. https://doi.org/10.1016/j.ultsonch.2017.11.036
24. Wei, J.; Shen, W. FeOOH quantum dot decorated flower-like WO_3 microspheres for visible light driven photo-Fenton degradation of Methylene Blue and Acid Red-18. *Colloids Surf. A Physicochem. Eng. Asp.* **2022**, 643, 128754. https://doi.org/10.1016/j.colsurfa.2022.128754
25. Kulštáková, A. Removal of pharmaceutical micropollutants from real wastewater matrices by means of photochemical advanced oxidation processes – a review *J. Water Process Eng.* **2023**, 53, 103727. https://doi.org/10.1016/j.jwpe.2023.103727
26. Bergendahl, J. A., Thies, T. P. Fenton's oxidation of MTBE with zero-valent iron. *Water Res.* **2004**, 38(2), 327-334.
27. Azizi, A., Moghaddam, M. R. A., Maknoon, R., Kowsari, E. Investigation of enhanced Fenton process (EFP) in color and COD removal of wastewater containing Acid Red 18 by response surface methodology: evaluation of EFP as post treatment. *Desalination Water Treat.* **2015**, 57(30), 1944-3994. https://doi.org/10.1080/19443994.2015.1063011
28. Garcia-Segura, S. Brillas, E. Combustion of textile monoazo, diazo and triazo dyes by solar photoelectro-Fenton: Decolorization, kinetics and degradation routes. *Applied Catalysis B: Environmental*, 2016, 181, 681–691. https://doi.org/10.1016/j.apcatb.2015.08.042
29. Gharaghani, M. A., Dehdarirad, A., Mahdizadeh, H., Hashemi, H., Nasiri, A., Samaei, M. R., Mohammadpour, A. Photocatalytic degradation of Acid Red 18 by synthesized $AgCoFe_2O_4$@Ch/AC: Recyclable, environmentally friendly, chemically stable, and cost-effective magnetic nano hybrid catalyst. *Int. J. Biol. Macromol.* **2024**, 269(1), 131897. https://doi.org/10.1016/j.ijbiomac.2024.131897
30. Vázquez-Vélez, E., Martínez, H., Castillo, F. Degradation of Acid Red 1 catalyzed by peroxidase activity of iron oxide nanoparticles and detected by SERS. *Nanomaterials* **2021**, 11(11), 3044. https://doi.org/10.3390/nano11113044
31. Ara, A., Khattak, R., Khan, M. S., Begum, B., Khan, S., Han, C. Synthesis, characterization, and solar photo-activation of chitosan-modified nickel magnetite bio-composite for degradation of recalcitrant organic pollutants in water. *Catalysts* **2022**, 12(9), 983. https://doi.org/10.3390/catal12090983
32. Hassan, H., Hameed, B. H. Oxidative decolorization of Acid Red 1 solutions by Fe-zeolite Y type catalyst. *Desalination* **2011**, 276, 45-52. https://doi.org/10.1016/j.desal.2011.03.018
33. Zare, M. R., Mengelizadeh, N., Aghdavodian, G., Zare, F., Ansari, Z., Hashemi, F., Moradalizadeh, S. Adsorption of Acid Red 18 from aqueous solutions by GO-$COFe_2O_4$: Adsorption kinetic and isotherms, adsorption mechanism and adsorbent regeneration. *Desalination Water Treat.* **2024**, 317, 100219. https://doi.org/10.1016/j.dwt.2024.100219
34. Santana, C. S., Ramos, M. D. N., Velloso, C. C. V., Aguiar, A. Kinetic evaluation of dye decolorization by Fenton processes in the presence of 3-Hydroxyanthranilic Acid. *Int. J. Environ. Res. Public Health* **2019**, 16(9), 1602. https://doi.org/10.3390%2Fijerph16091602
35. Liang, X., Zhong, Y., Zhu, S., Zhu, J., Yuan, P., He, H., Zhang, J. The decolorization of Acid Orange II in non-homogeneous Fenton reaction catalyzed by natural vanadium–titanium magnetite. *J. Hazard. Mater.* **2010**, 181(1-3), 112-120. https://doi.org/10.1016/j.jhazmat.2010.04.101
36. Zhao, Q., Zhang, C., Tong, X., Zou, Y., Li, Y., Wei, F. Fe_3O_4-NPs/orange peel composite as magnetic heterogeneous Fenton-like catalyst towards high-efficiency degradation of methyl orange. *Water Sci. Technol.* **2021**, 84(1), 159–171. https://doi.org/10.2166/wst.2021.221

37. Nguyen, X. S., Ngo, K. D. The role of metal-doped into magnetite catalysts for the photo-Fenton degradation of organic pollutants. *J. Surf. Eng. Mater. Adv. Technol.* **2018**, 8(1). https://doi.org/10.4236/jsemat.2018.81001
38. Choe, Y. J., Kim, J., Byun, J. Y., Kim, S. H. An electro-Fenton system with magnetite coated stainless steel mesh as cathode. *Catal. Today* **2021**, 359, 16-22. https://doi.org/10.1016/j.cattod.2019.06.062
39. Abou-Gamra, Z. M. Kinetic and thermodynamic study for Fenton-like oxidation of Amaranth Red dye. *Adv. Chem. Eng. Sci.* **2014**, 4(3), 285-291. http://dx.doi.org/10.4236/aces.2014.43031
40. Shuchi, S. B.; Suhan, M. B. K.; Humayun, S. B.; Haque, M. E.; Islam, M. S. Heat-activated potassium persulfate treatment of Sudan Black B dye: Degradation kinetic and thermodynamic studies. *J. Water Process Eng.* **2021**, 39, 101690. https://doi.org/10.1016/j.jwpe.2020.101690
41. Ball, P., Nicholls, C. H. Azo-hydrazone tautomerism of hydroxyazo compounds-a review. *Dyes Pigm.* **1982**, 3(1), 5-26.
42. Omura, T.; Kayane, Y.; Tezuka, Y. Design of chlorine-fast reactive dyes: Part 1: The role of sulphonate groups and optimization of their positions in an arylazonaphthol system. *Dyes Pigm.* **1992**, 20(4), 227-246.
43. Zhang, G.; Zhang, S. Quantitative structure-activity relationship in the photodegradation of azo dyes. *J. of Environmental Sci.* **2020**, 90, 41-50. https://doi.org/10.1016/j.jes.2019.11.009.
44. Pearson, R. G. Hard and soft acids and bases. *J. Am. Chem. Soc.* **1963**, 85(22), 3533-3539.
45. Dai, H., Xu, S., Chen, J., Miao, X., Zhu, J. Oxalate enhanced degradation of Orange II in heterogeneous UV-Fenton system catalyzed by Fe_3O_4@g-Fe_2O_3 composite. *Chemosphere* **2018**, 199, 147-153. https://doi.org/10.1016/j.chemosphere.2018.02.016
46. Paz, C. B.; Araújo, R. S.; Oton, L. F.; Oliveira, A. C.; Soares, J. M.; Medeiros, S. N.; Rodríguez-Castellón, E.; Rodríguez-Aguado, E. Acid Red 66 dye removal from aqueous solution by Fe/C-based composites: Adsorption, kinetics and thermodynamic studies. *Mater.* **2020**, 13(5), 1107). https://doi.org/10.3390/ma13051107
47. Gurushankar, K., Chinnaiah, K., Kannan, K., Gohulkumar, M., Periyasamy, P. Synthesis and characterization of FeO nanoparticles by hydrothermal method. *Rasayan J. Chem.* **2021**, 14(3), 1985-1989. http://doi.org/10.31788/RJC.2021.1436299
48. Martina, M. R.; Zoli, L.; Sani, E. Synthesis and characterization of goethite (α-FeOOH) magnetic nanofluids. *Int. J. Thermofluids* **2022**, 15, 100169. https://doi.org/10.1016/j.ijft.2022.100169
49. Abo-Farha, S. A. Comparative study of oxidation of some azo dyes by different advanced oxidation processes: Fenton, Fenton-Like, photo-Fenton and photo-Fenton-like. *J. Am. Sci.* **2010**, 6(10), 128-142.
50. Lucas, M. S.; Algarra, M.; Jiménez-Jiménez, J.; Rodríguez-Castellón, E.; Peres, J. A. Catalytic activity of porous phosphate heterostructures-Fe towards Reactive Black 5 degradation. *Int. J. Photoenergy* **2013**, 2013, 1-6. https://doi.org/10.1155/2013/658231
51. Chen, K., Wang, G., Li, W., Wan, D., Hu, Q., Lu, L. Application of response surface methodology for optimization of Orange II removal by heterogeneous Fenton-like process using Fe_3O_4 nanoparticles. *Chin. Chem. Lett.* **2014**, 25(11), 1455-1460. https://doi.org/10.1016/j.cclet.2014.06.014
52. Fu, F., Wang, Q., Tang, B. Effective degradation of C.I. Acid Red 73 by advanced Fenton process. *J. Hazard. Mater.* **2010**, 174, 17-22. https://doi.org/10.1016/j.jhazmat.2009.09.009
53. Faria, A. J. M.; Silva, A. N.; Oliveira, A. C.; do Carmo, J. V. C.; Saraiva, G. D.; Juca, R. F.; Morales, M. A.; Lang, R.; Jiménez, J. J.; Rodríguez-Castellón, E. Catalytic performances of the nano FeCo solids for biofuel additives production: Incorporation of promoters effects on the stability of the catalysts. *Energy & Fuels* **2023**, 37, 22, 17328–17344. https://doi.org/10.1021/acs.energyfuels.3c02881
54. Rajan, A.; Sharma, M.; Sahu, N. S. Assessing magnetic and inductive thermal properties of various surfactants functionalised Fe_3O_4 nanoparticles for hyperthermia. *Sci. Rep.* **2020**, 10, 15045. https://doi.org/10.1038/s41598-020-71703-6
55. Zhong, Y.; Yu, L.; Chen, Z.-F.; He, H.; Ye, F.; Cheng, G.; Zha, Q. Microwave-assisted synthesis of Fe_3O_4 nanocrystals with predominantly exposed facets and their heterogeneous UVA/Fenton catalytic activity. *ACS Appl. Mater. Interfaces* **2017**, 9, 29203–29212. https://doi.org/10.1021/acsami.7b06925
56. Ai, Q.; Yuan, Z.; Huang, R.; Yang, C.; Jiang, G.; Xiong, J.; Huang, Z.; Yuan, S. One-pot co-precipitation synthesis of Fe_3O_4 nanoparticles embedded in 3D carbonaceous matrix as anode for lithium ion batteries. *J. Mater. Sci.* **2019**, 54, 4212–4224. https://doi.org/10.1007/s10853-018-3141-3
57. Yamashita, T.; Hayes, P. Analysis of XPS spectra of Fe^{2+} and Fe^{3+} ions in oxide materials. *Appl. Surf. Sci.* **2008**, 254, 2441-2449. https://doi.org/10.1016/j.apsusc.2007.09.063
58. Klassen, N. V., Marchington, D., McGowan, H. C. E. H_2O_2 determination by the I_3^- method and by $KMnO_4$ titration. *Analytical Chem.* **1994**, 66(18), 2921-2925.
59. Liu, X.; Zhao, T.; Liu, P.; Cui, P.; Hu, P. Manufacture of nano graphite oxides derived from aqueous glucose solutions and in-situ synthesis of magnetite graphite oxide composites. *Mater. Chem. Phys.* **2015**, 153, 202-208. https://doi.org/10.1016/j.matchemphys.2015.01.004

 doi:10.20944/preprints202408.0535.v1

60. Quiñones-Murillo, D. H.; Ariza-Reyes, A. A.; Ardila-Vélez, L. J. Some kinetic and synergistic considerations on the oxidation of the azo compound Ponceau 4R by solar–mediated heterogeneous photocatalytic ozonation. *Desalin. Water Treat.* **2019**, 170, 61-74. https://doi.org/10.5004/dwt.2019.24711
61. Hashemian, S. Fenton-like oxidation of Malachite Green Solutions: Kinetic and thermodynamic study. *J. Chem.* **2013**, 2013, 1-7. https://doi.org/10.1155/2013/809318